Electrochemical and hydraulic analysis of thin-film composite and cellulose triacetate membranes for seawater electrolysis applications

Rachel Taylor [a], Le Shi [b,c], Xuechen Zhou [b], Ruggero Rossi [d], Cristian Picioreanu [e], Bruce E. Logan [a,b,*]

[a] Department of Chemical Engineering, The Pennsylvania State University, University Park, PA, USA
[b] Department of Civil and Environmental Engineering, The Pennsylvania State University, University Park, PA, USA
[c] Key Laboratory of Environment Remediation and Ecological Health, Ministry of Education, College of Environmental and Resource Sciences, Zhejiang University, Hangzhou, PR China
[d] Department of Environmental Health and Engineering, Johns Hopkins University, Baltimore, MD, USA
[e] Water Desalination and Reuse Center (WDRC), Biological and Environmental Science and Engineering Division (BESE), King Abdullah University of Science and Technology (Thuwal, Saudi Arabia

ARTICLE INFO

ABSTRACT

Polymeric filtration membranes could be a cost-effective alternative to cation exchange membranes (CEMs) in electrolysis with a contained anolyte and saltwater catholyte because they size selectively hinder salt ion transport between compartments while facilitating proton and hydroxide transport. Optimizing membrane performance requires a better understanding of membrane properties that impact electrical resistances and ion retention. Twelve reverse osmosis (RO) membranes, one nanofiltration (NF) membrane, and one cellulose triacetate forward osmosis (FO) membrane were examined for their electrical resistances under conditions typically used for characterization of CEMs. Resistances measured at low current densities (0.07–0.3 mA cm^{-2}) varied between different membranes by over an order of magnitude in 1 M NaCl at neutral pH, from 6.1 ± 0.1 Ω cm^2 to 70 ± 30 Ω cm^2. There was no significant correlation between membrane resistance and applied potential during saltwater electrolysis at 20 mA cm^{-2} (p = 0.44), or between membrane resistance and water permeability (p = 0.35). These results indicate that traditional CEM resistance characterization methods do not predict polymeric filtration membrane electrolysis performance because proton and hydroxide transport, which is important during electrolysis when large pH gradients develop, must be considered separately from salt ion and water molecule transport through size selective RO, NF, and FO membranes during water electrolysis.

1. Introduction

Ultra-pure water is currently required for water electrolysis to produce carbon neutral (green) hydrogen through proton exchange membrane (PEM) electrolysis [1–3]. Research into using less purified water is gaining momentum because low-grade waters such as brackish water or seawater are more globally accessible, while coastal regions, where seawater is available, typically have better access to renewable energy sources compared to onshore locations. Additionally, producing highly deionized water makes the overall process more complex and expensive [4,5]. Direct seawater electrolysis has been difficult to implement due to the presence of chloride ions in seawater which react at the anode to form undesirable species such as chlorine and derivative species (e.g.

hypochlorite and hypochlorous acid), which can damage electrolyzer components [6]. While there has been extensive research into developing novel catalysts that preferentially evolve oxygen over chlorine, an alternative approach is using thin-film composite reverse osmosis (RO) membranes with a contained anolyte and a seawater catholyte [7–12]. An anolyte that contains fully oxidized salt species such as perchlorate (NaClO$_4$) can be used as an inert electrolyte, while the membrane prevents chloride ion transfer to the anode and thus its oxidation to chlorine gas and other species. Traditional cation exchange membranes (CEMs) cannot be used under these conditions because they allow too much chloride ion leakage from the catholyte to the anolyte [1]. RO membranes have an additional advantage of being substantially less expensive than CEMs [12].

RO, forward osmosis (FO), and nanofiltration (NF) membranes are three types of size-selective membranes that are being studied as alternatives to ion exchange membranes. RO membranes have the greatest selectivity for preventing transport of salt species, but they must facilitate transport of small ions, such as protons/hydronium and hydroxide, to maintain the high current densities needed in water electrolyzers [13–16]. RO, NF, and FO membranes are size selective due to their highly dense active layers [17–19]. Thin film composite RO and NF membranes are typically composed of three layers, including a dense, polyamide active layer, which can range between 20 and 150 nm thick for NF membranes and 100–200 nm thick for RO membranes [20]. The active layer is bound to a polysulfone support layer (~50 μm) which is used to connect the thin, fragile active layer to a thick (~100 μm) polyester web backbone. The polyester web backbone maintains the mechanical properties of the membranes in large hydraulic pressure gradients [14,21,22]. While FO membranes also have a size-selective active layer, they differ in that a porous support layer is not required to have mechanical strength to withstand higher pressures because water transport across FO membranes is only driven by an osmotic pressure gradient [23]. CEMs are usually homogenous block co-polymers, charged to selectively transport all cations in a solution with only a small dependence on the size of the ions. However, RO, NF, and FO membranes mainly transport species based on size, which allows for the selective containment of large salt ions in the anolyte and catholyte while transporting protons and hydroxide ions to maintain a set current density [24]. The electrochemical properties of RO, NF, and FO membranes have yet to be broadly studied for applications in electro-driven separations such as saltwater electrolysis.

In electro-driven processes, membrane electrical resistance is one of several factors used to compare electrolyzer performance [24–26]. Electrical resistance is a measure of a membrane's ability to transport electrical charge in the form of ions across it, and therefore ion exchange membranes with higher resistances increase energy consumption for water electrolysis [24,26]. The electrical resistance of the RO membrane active layer has been measured using electrochemical impedance spectroscopy and has been related to salt permeability during desalination tests with a large water flux through the membrane. Few studies have examined the resistance of the RO membrane active layer and supporting layers together, which is the critical property of these membranes in electrochemical applications [15,27–29]. In the first study using RO membranes for water electrolyzers, Shi et al. [12] showed that one RO membrane had an electrical resistance comparable to CEMs, while another had a much larger electrical resistance. The membrane with a resistance comparable to the CEM was used to electrolyze saltwater at an applied potential similar to that used with the CEM, while using the membrane with the higher resistance required a higher applied potential during electrolysis, but the reason for this difference in performance between the two RO membranes was not reported [12]. Because only two RO membranes were used, it was not possible to examine if other membrane properties, such as water permeability, could be used to predict performance in a water electrolyzer [12].

The purpose of this study was to determine if resistances of different size-selective filtration membranes, measured under conditions typically used to characterize resistances of CEMs, could be correlated with water electrolyzer performance at high current densities. At high current densities, large pH gradients develop, and water ions account for a larger percentage of charge transport across the membrane, while in low current density resistance tests, salt ions primarily transport charge across the membrane. Electrical resistances were measured at a low current density in neutral pH for twelve RO membranes, one NF membrane, and one FO membrane. Three RO membranes with varying electrical resistances, and the FO and NF membranes were selected for further characterization in electrolyzer and permeability tests to examine whether water flux could be used to better understand membrane performance in water electrolyzers. Therefore, membrane overpotential, salt ion crossover during electrolysis, and membrane permeability were examined to see if any of these properties could be correlated to membrane resistance or be used to determine optimal characteristics of TFC membranes for green hydrogen production from saltwater.

2. Experimental

2.1. Membranes

The following flat-sheet RO membranes were used (membrane abbreviations in parentheses) based on the manufacturer and intended application of either brackish water (BW) or seawater (SW) desalination: Trisep Membrane ACM5 [RO1 (BW)]; DuPont membranes BWXLE [RO2 (BW)], BW30XLE [RO4 (BW)], SWXLE [RO5 (SW)], BW30 [RO6 (BW)], BW30LE [RO7 (BW)]; Hydranautics membranes SWC4 [RO3 (SW)], SWC5 [RO8 (SW)]; Toray membranes 73AC [RO9 (BW)], 73HA [RO10 (BW)]; GE Suez membranes GE AK [RO11 (BW)], GE AG [RO12 (BW)]. The nanofiltration membrane was DuPont NF270 (NF), and the forward osmosis membrane was Fluid Technology Solutions CTA FO (FO). A variety of RO membranes with different rejections, manufacturers, and advertised energy requirements were studied to understand how much RO membrane electrochemical performance can vary. An outside micrometer (Mitutoyo Kawasaki, Japan) was used to measure the total thickness of dry membranes.

2.2. Resistance measurements

The membrane resistances were determined using a four-electrode direct current method typically employed for CEMs [12,30,31]. The electrodes and membrane were submerged in 60 mL of electrolyte solution, in a cylindrical chamber with a cross-sectional area of 7 cm^2. The membrane was positioned in the middle of the chamber, 5 cm away from the anode and cathode. A scheme and picture of the experimental set-up is in the supporting information (Supporting Information, Fig. S1 and Fig. S2). Platinum coated titanium mesh electrodes were used as the anode and cathode, placed 10 cm apart. Two Ag/AgCl (3 M NaCl) reference electrodes (BASi West Lafayette, IN) with Luggin capillaries were placed on either side of the membrane. The Luggin capillaries minimized the ohmic drop between the reference electrodes [32]. The exposed membrane area, 7 cm^2, was the same as the cross section of the cylindrical chamber.

A potentiostat (Biologic VMP3) was used to obtain linear sweep voltammetry (LSV) data from 0 V to 3.5 V at a scan rate of 5 mV/s. From this data, the ohmic region was determined, and current densities were selected for membrane electric resistance measurements. In the ohmic region, the applied potential, U (V), changes linearly with current, I (A), and the proportionality constant between the two is the ohmic resistance R (Ω), consistent with Ohm's law, $U = IR$ [33]. Measuring the potential across a membrane at current densities in the ohmic region will yield the ohmic resistance of the membrane as the slope of the potential vs. current data. Eight current densities were selected that ranged from 0.07 to 0.3 mA cm^{-2} in chronopotentiometry (CP) tests based on 30 s intervals. An example of how resistance is calculated from chronopotentiometry data is provided in the SI.

Membrane resistance (R_{mem}) was calculated from measurements made in the absence and presence of the membrane, based on $R_{mem} = R_{sol+mem} - R_{sol}$, where R_{sol} (the solution resistance measured without membrane) was subtracted from the total resistance with the membrane present, $R_{sol+mem}$. The area resistance (Ω cm^2) of the membrane was calculated using the exposed membrane area. Measurements were repeated 3 times, using a fresh piece of membrane each time. The resistances for each membrane were measured in both 0.6 M (~3.5 wt%) and 1 M (~5.5 wt%) NaCl. The membranes were equilibrated in the electrolyte for three days prior to the experiment.

2.3. Water flux measurements

The water flux through the membrane was measured using a high-pressure dead-end cell (HP 4759, Sterlitech, Auburn, WA). Deionized water was used at an applied pressure of 34.4 bar. The mass of permeate was measured over time using a scale, and this data was used to calculate the flux normalized to pressure (L m^{-2} h^{-1} bar^{-1} or, usually written as LMH bar^{-1}). The exposed membrane area was 14.6 cm^2.

2.4. Water electrolyzer experiments

The applied cell potentials required for saltwater electrolysis with an asymmetric anolyte and catholyte contained by each membrane was compared at a constant current. A zero-gap electrolyzer (Scribner, North Carolina) configuration was used to investigate performance in a conventional proton exchange membrane (PEM) electrolyzer [34,35]. In the zero-gap electrolyzer, the membrane is placed directly next to the anode and cathode to minimize ohmic resistance. The anode and cathode are placed adjacent to serpentine flow channels carrying the anolyte and catholyte at a rate of 15 mL s^{-1}. A platinized titanium (Pt-Ti) flow field is used for the anode and a graphite flow field is used for the cathode. Gold plated copper current collectors are attached to the Pt–Ti and graphite flow fields, and all components are contained between two exterior anodized aluminum end plates held together with bolts and washers.

A two-electrode set-up was used to perform the experiment and measure the applied potential required for saltwater electrolysis. Carbon cloth electrodes (4 cm^2) coated with 10% Pt/C catalyst were used as the anode and cathode. The anolyte was 1 M NaClO$_4$ and catholyte was 1 M NaCl with the electrolytes (each 200 mL) recirculated through the flow cell at a rate of 15 mL s^{-1}. The exposed membrane area was 5 cm^2. Chronopotentiometry (CP) was used at a constant current density of 20 mA cm^{-2} using a potentiostat. Experiments were run for 3 h, and the applied potentials were compared at the end of the 3 h. Each experiment was conducted twice for each membrane type, using a fresh piece of membrane and fresh electrodes each time (n = 2).

2.5. Ion crossover experiments

A two-electrode set-up was used to measure ion transport across the membranes, as previously described [12]. The anode and cathode were both carbon paper coated with a 10% platinum/carbon catalyst and had areas of 1.68 cm^2. The catholyte was 30 mL of 1 M KCl, and the anolyte was 30 mL of 1 M NaClO$_4$. K$^+$ was used in the catholyte so the Na$^+$ crossover could be studied in the direction of the electric field. The anolyte and catholyte were added into the cylindrical cell, and CP was used to apply a current density of 10 mA cm^{-2} for 1 h to facilitate electrolysis. After this step the anolyte and catholyte were collected, the pH of both were measured, and ion chromatography (Dionex, Thermo Fisher Waltham, MA) was used to measure the concentration of ions that crossed over into each compartment, (Na$^+$ and ClO$_4^-$ in the catholyte, or K$^+$ and Cl$^-$ in the anolyte). The membrane had an exposed area of 7 cm^2.

3. Results and discussion

3.1. Membrane resistances

Membrane resistances varied by an order of magnitude with no apparent correlation between resistance and the type of RO membrane (BW or SW). In 1 M NaCl, the RO1 (BW) membrane had the lowest resistance of 6.1 $\pm$ 0.1 Ω cm^2, an order of magnitude lower than the RO9 (BW) membrane, with the highest resistance of 70 $\pm$ 30 Ω cm^2 (Fig. 1). BWRO and SWRO membranes had similar resistances, despite their different reported salt rejections and permeabilities [36]. The NF membrane had a NaCl rejection much lower than all the RO membranes (50% compared to 98.5–99.8%) according to manufacturer data, and one of the lowest measured resistances in 1 M NaCl, 14 $\pm$ 1.7 Ω cm^2
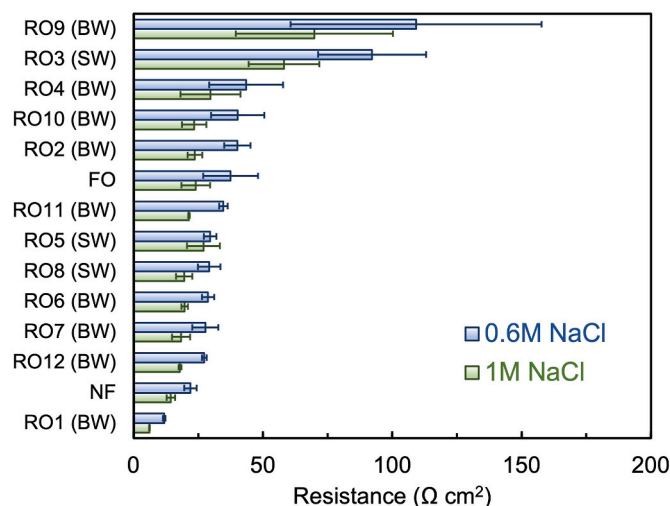

Fig. 1. Resistances of RO, NF, and FO membranes measured in either 0.6 M or 1 M NaCl using the four-electrode direct current method.

[37]. A BWRO membrane with a reported salt rejection of 98.5% had an even lower resistance (RO1), suggesting that the same properties that control one directional ion transport during water filtration do not control two directional ion transport across membranes in potential gradient [38,39]. The FO membrane had a resistance of 24 $\pm$ 5.6 Ω cm^2, which was in the midrange in comparison to the other membrane resistances.

On average, the resistances of the membranes increased by 35 $\pm$ 8% from the 1 M–0.6 M NaCl solution, suggesting there is a proportional relationship between electrolyte concentration and conductivity, as a 40% decrease in concentration resulted in a 35 $\pm$ 8% increase in conductivity. This decrease in membrane resistance reflects the decrease in the number of charge carriers present in lower concentration solutions.

One potential reason for the observed weak correlation between electrical resistance and membrane type (BWRO, SWRO, NF, FO) is due to the membrane support layers influencing their resistances. In general, membrane resistance is directly related to both material resistivity and thickness [40]. The membrane backbone, which minimally contributes to membrane filtration performance, might still have a significant ohmic contribution during resistance measurements due to its large thickness (~150 μm), about a thousand times larger than the polyamide active layer thickness (~150 nm) [41]. Although the resistivities have not been reported for dense polyamide and polyester web backbone, their porosities (less than 20% for PA [42,43] and greater than 60% for polyester web [44,45]) suggest the polyamide layer will have a higher resistivity than the polyester support layer. Thus, the thickness of the backbone layers could bring its resistance to values comparable to that of the polyamide layer. Therefore, while the support layers minimally contribute to salt selectivity during filtration [15], they might be responsible for the electrical resistance and thus not correlate with filtration parameters and membrane type (SWRO, BWRO, NF, or FO). Further measurements of the backbone resistance will quantify its ohmic contribution in comparison to the total membrane thickness.

The large variations observed for the membranes with high resistances may be reflective of measurements of very small amounts of ion flux across the membrane. When the membrane resistance is high, the salt passage is low, and a small increase in salt passage is equivalent to a large fractional increase. Previous studies reporting membrane resistance with this method also reported large error bars for their highest resistance membranes [12].

The total membrane thickness did not have any correlation with the membrane resistance (p = 0.5, Supporting Information, Fig. S5). Membrane resistance is directly proportional to the total thickness of a single type of homogenous CEM, enabling trends between CEM resistance and

membrane thickness [46,47]. However, the situation for other types of membranes is more complicated due varying properties of the three layers. When we compared the total thickness of the RO, NF and FO membranes to their membrane resistance we found no significant trend. This indicated that the layers have thicknesses and permeabilities that vary for each membrane type and influence the overall resistance to charge transfer [17].

3.2. Water permeabilities

Membrane permeabilities ranged from 0.7 L m^{-2} h^{-1} bar^{-1} (RO3) to 14.6 L m^{-2} h^{-1} bar^{-1} (NF) (Fig. 2a). There was a general increase in resistance with less water permeability, but there was no significant trend ($y = 20.97e^{-0.04x}$, $R^2 = 0.67$, $p = 0.35$) (Fig. 2b). The permeabilities of three RO membranes with varying electrical resistances were measured, as well as the nanofiltration membrane due to its different composition. The FO membrane permeability was not measured because the membrane is only used with an osmotic pressure gradient and thus it cannot withstand the high hydraulic pressure used in the test. The measured NF membrane permeability was comparable to that reported in literature (Fig. 2a) [48,49]. NF membranes have larger pore sizes (0.5–2 nm) than RO membranes (0.2–1 nm) because they are typically
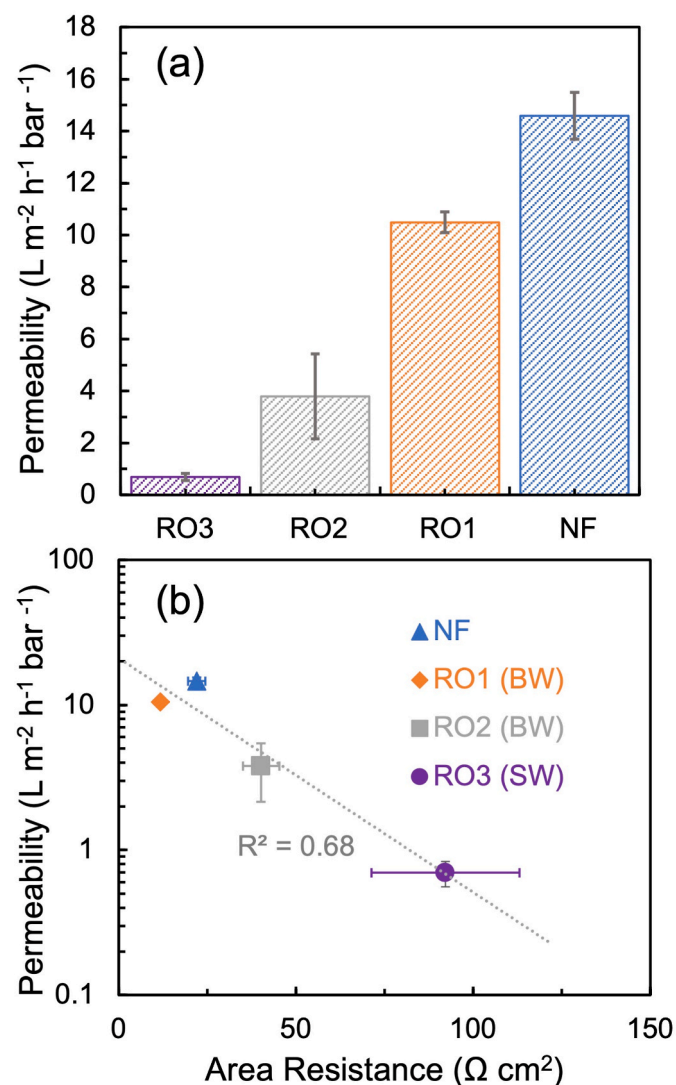
used to filter organic compounds and soften surface and groundwater by separating divalent ions [38,50–52]. Therefore, NF membranes have higher water and NaCl permeability than RO membranes. SWRO membranes are typically used in higher pressure gradients with higher concentration salt solutions, so they have higher salt rejections and lower permeabilities to achieve the desired separation [53]. Thus, it is reasonable the SWRO membrane has the lowest water permeability of the four membranes measured. When only the RO membrane permeabilities were plotted against their electric resistance, the fitted curve had $R^2 = 1$ but the trend was not significant ($p = 0.08$) possible due to the limited number of data points.

3.3. Membrane performance in electrolysis

Membranes with higher resistances required higher voltage during saltwater electrolysis, but statistically, membrane resistance and applied potential required for saltwater electrolysis could not be shown to be significantly correlated ($R^2 = 0.38$, $p = 0.44$) (Fig. 3b). Electrolyzing
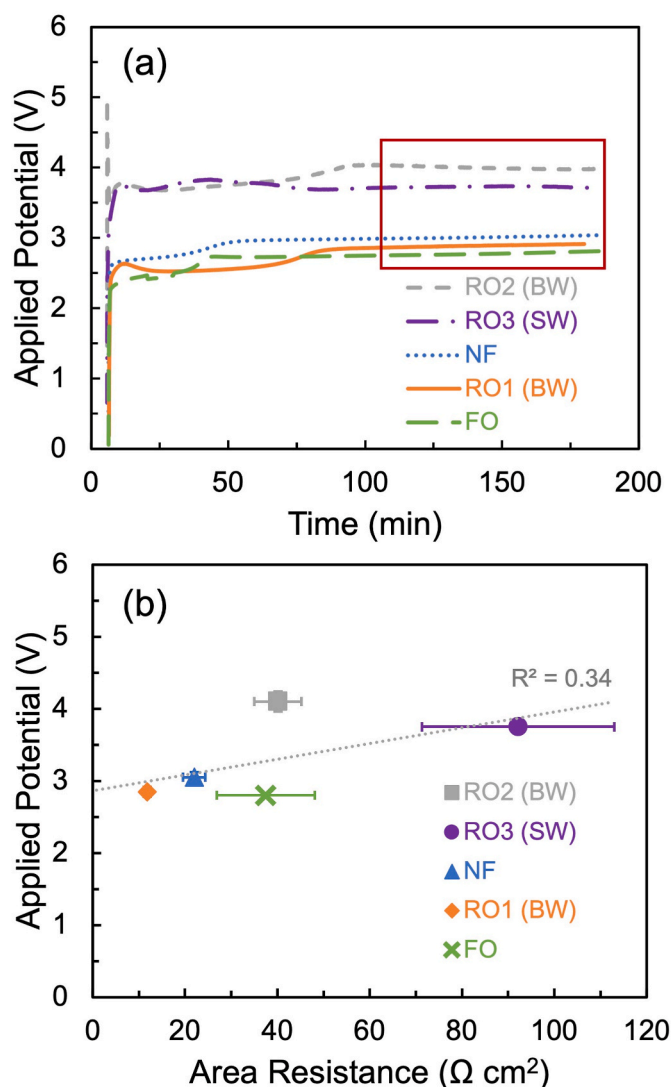

Fig. 2. (a) Water permeabilities of three RO membranes and one NF membrane measured at an applied pressure of 34.4 bar. (b) Water permeabilities as a function of measured area resistance.

Fig. 3. (a) Potential applied to electrolyze saltwater at a constant current density of 20 mA/cm^2 for 3 h using three RO membranes, one NF membrane, and one FO membrane. The applied potential was compared when it had stabilized after 2 h, indicated by the red box. **(b)** Comparison of the applied potentials for saltwater electrolysis and the membrane resistances. The equation of the line is $y = 0.01x + 2.87$. (For interpretation of the references to colour in this figure legend, the reader is referred to the Web version of this article.)

saltwater with the FO membrane required the smallest applied potential of 2.8 ± 0 V, although this membrane did not have the smallest measured resistance (Fig. 3a). The membrane with the smallest measured resistance, RO1 (BW), had a similar applied potential of 2.9 ± 0.1 V. Electrolysis with the RO2 (BW) membrane required the highest applied potential of 4.1 ± 0.1 V, while the RO3 (SW) membrane, which had the largest measured membrane resistance, had an applied potential of 3.8 ± 0.1 V. The membrane resistances in 0.6 M NaCl were plotted against the applied potential required for electrolysis using each membrane (Fig. 3b). The lack of a correlation contrasts with trends amongst traditional ion exchange membranes, where membrane resistance at low current directly correlates to applied potential in electrochemical cells [26,54].

The generation of protons at the anode and hydroxide ions at the cathode during water electrolyzer tests produced large pH gradients between the electrolytes [12]. The final pHs after 3 h of electrolysis (Supplementary Information, Fig. S7) were 1.4 ± 0.1 for the anolyte and 12.2 ± 0.1 for the catholyte. RO and NF membranes can tolerate this pH range; however, the pH operating range of FO membranes is 3–7 [51,55,56]. Contact with the acidic anolyte and basic catholyte may have damaged the membrane, resulting in a lower applied potential being required for this membrane [55,57].

3.4. Membrane ion crossover

In resistance tests at neutral pH (at low current densities), the concentrations of H^+ and OH^- are very low so charge is balanced by salt ions transported through the RO membrane. However, during water electrolysis large pH gradients develop, so water ion migration plays a larger role in current transport across the membrane. The difference between salt ion flux and proton or hydroxide ion flux is more significant in RO, NF, and FO membranes than in CEMs because of their steric partitioning in addition to dielectric and Donnan partitioning [58,59]. While it is possible to correlate neutral membrane resistance to applied potential during electrolysis for CEMs, it was not possible to correlate these two properties for RO, NF, and FO membranes.

RO, NF, and FO membranes hinder proton and hydroxide transport differently than they hinder Na^+ and Cl^- transport because of their dense, size selective active layers with pore sizes between 0.1 and 2 nm [50]. Electrochemical impedance spectroscopy (EIS) was reported to measure the conductance of the active layer of RO membranes in pH 3.7 and 5.7 salt solutions (both KCl and MgCl) using a rotating disk electrode [27]. The active layer had a higher conductance in the solution with a higher concentration of protons (pH 3.7). The EIS study differs from this one in that it considers only the active layer of the membrane, but similar trends are observed when comparing the total membrane resistance in neutral solution to applied potential during electrolysis with large pH gradients. Protons can more easily transport and carry current across the dense polyamide layer, so increasing their concentration during electrolysis changes the membrane resistance to charge transfer in comparison to the neutral salt solution.

To demonstrate the relative importance of salt ion versus water ion transport in water electrolyzer tests salt ion crossover was measured using electrolytes with four different salt ions. The catholyte contained KCl and the anolyte was $NaClO_4$. Na^+ crossover was higher for the FO (49.5 ± 0.5 mM) and NF (27.3 ± 0.04 mM) membranes than for the RO membranes (RO1 = 4.4 ± 0.5 mM, RO2 = 5.3 ± 0.5 mM, RO3 = 9.8 ± 0.7 mM) (Fig. 4). Conversely, Cl^- crossover was higher for the RO membranes than for the NF and FO membranes. For Cl^- crossover, RO1 (BW) had 23.0 ± 0.7 mM, RO2 (BW) had 21.0 ± 0.2 mM, and RO3 (SW) had 10.5 ± 0.2 mM. For the NF and FO membranes Cl^- crossover was about four times less, with NF having 6.5 ± 0.01 mM and FO having 5.5 ± 0.6 mM. K^+ and ClO_4^- crossover was one to two orders of magnitude less than Na^+ and ClO_4^- crossover. The FO membrane had the highest amount of K^+ crossover (7.5 ± 0.4 mM), and the K^+ crossover for RO2, and RO3 was undetectable. The ClO_4^- crossover followed a similar trend as the Na^+ crossover, with the FO and NF membranes having the most crossover (FO = 7.3 ± 0.1 mM, NF = 4.3 ± 0.1 mM), and the RO membranes having the least crossover (RO1 = 0.47 ± 0.07 mM, RO2 = 0.36 ± 0.01, RO3 = 0.44 ± 0.01).

Na^+ and Cl^- ions are transported across the membrane in the same direction as the electric field, and so their transport is due to both diffusional and electromigration forces. Thus, these two ions had the highest amount of crossover for all membranes. RO membranes showed higher Cl^- crossover than Na^+, while the FO and NF membranes had more Na^+ crossover than Cl^-. The RO and NF membranes had their
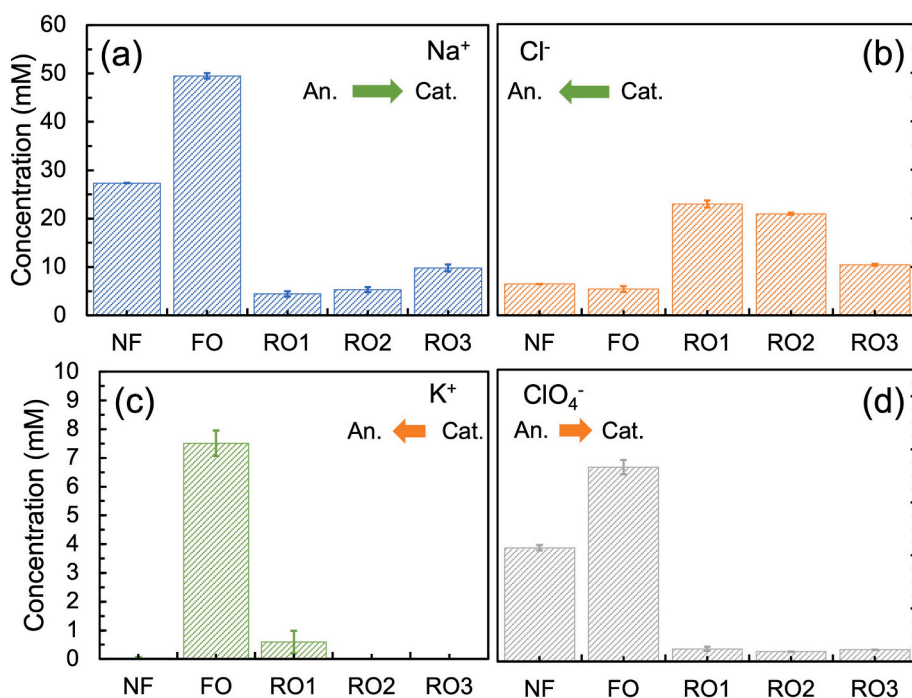

Fig. 4. Concentration of salt ions that crossed over the membrane after a current density of 20 mA cm^{-2} was applied to the cylindrical reactor for 1 h with 1 M NaClO$_4$ anolyte and 1 M KCl catholyte. Concentrations of ions that crossed over into the opposite chamber **(a)** sodium, **(b)** chloride, **(c)** potassium ions, and **(d)** perchlorate. Green arrows indicate ions with concentration and potential gradients in the same direction, while orange arrows indicate ions with concentration and potential gradients in opposite directions. RO 1 and 2 are BW membranes, RO 3 is an SW membrane. (For interpretation of the references to colour in this figure legend, the reader is referred to the Web version of this article.)

active layers facing the anolyte during the experiments. The proton generation at the anode caused an anolyte pH between 1 and 2 for all the membranes, (Supplementary Information, Fig. S8). According to published zeta potential data of RO membrane active layers, the active layer of the membrane is most likely positively charged at a pH between 1 and 2 [28]. During electrolysis, this positively charged active layer in contact with the acidic anolyte could have caused the preferential transport of Cl^- over Na^+ in the direction of the potential gradient [28]. Hydroxide generation at the cathode resulted in a pH between 12 and 13 in the catholyte (Supplementary Information, Fig. S8). By changing the active layer to face the catholyte instead of the anolyte, the membrane charge will most likely be negative instead, and Cl^- transport could be further reduced in comparison to Na^+ transport, as suggested by results in a previous study where the impact of the direction of active layer was examined on salt ion transport [12]. There was minimal K^+ and ClO_4^- crossover here for all membranes because the concentration and potential gradients for these ions were in directions opposite to the electric field.

Using the ion crossover data and the total Coulombs of charge passed through the electrolyzer based on the set current, we calculated the fraction of charge carrier that was due to water ions (protons and hydroxide ions) for each membrane (calculations in the Supplementary Information). The membranes with the lowest fraction of charge carrier (FO and NF) across the membrane had the highest amount of salt transport in the direction of the potential gradient which balanced charge across the membrane (Fig. 5a). The RO membranes hindered salt ion transport during electrolysis more so than the NF and CTA FO membranes. The FO membrane had the highest amount of total salt crossover, and RO3 (SW) had the least amount of total salt crossover and highest fraction of proton and hydroxide charge carriers.

The FO membrane has a more homogenous active layer than a typical RO membrane with higher free volume, making it a looser membrane, so salt ion transport across the membrane could rapidly occur (even during the brief few minutes when the chronopotentiometry experiment was being set up and initial salt samples were being collected), causing this membrane to have a fraction of charge carrier for protons and hydroxide close to zero [60]. Also, the FO membrane may have been damaged during electrolysis due to its smaller tolerance for a very high or low pH, which could have allowed salt ions to easily move between compartments during sample collection after the experiment. The smaller pore sizes and higher salt rejections of RO membranes may have contributed to them hindering ion transport more effectively than the NF and FO membranes [37]. The RO3 (SW) membrane has the highest reported salt rejection according to manufacturer spec sheets and the highest measured membrane resistance to Na^+ and Cl^- transport, indicating the membrane sufficiently hindered the salt transport and preferentially transported the electrochemically active species (protons and hydroxide ions).

The fraction charge carrier of protons for each membrane had an inverse trend with membrane permeability. The RO3 (SW) membrane had the lowest permeability and had the highest fraction of proton and hydroxide as charge carriers, while the membrane with the highest permeability (NF) had the lowest fraction of proton and hydroxide as charge carriers (Fig. 5b). This trend indicates that the membranes that most effectively hindered salt ion transport resulted in the charge being balanced by increased proton or hydroxide transport, although likely this trend was not significant ($R^2 = 0.82$, p = 0.13), which may be due to the small number of data (four membranes).

In contrast to the membrane resistance measurements done at neutral pH, the ion crossover experiments have large pH gradients between the anolyte and catholyte. The protons and hydroxide ions generated at the anode and cathode, respectively, are most likely minimally hindered by the thin-film composite membranes, and can easily carry charge across them, contributing to the set current density. These molecules are the smallest and have the largest diffusion coefficient in water of the ions present, making them the preferred charge
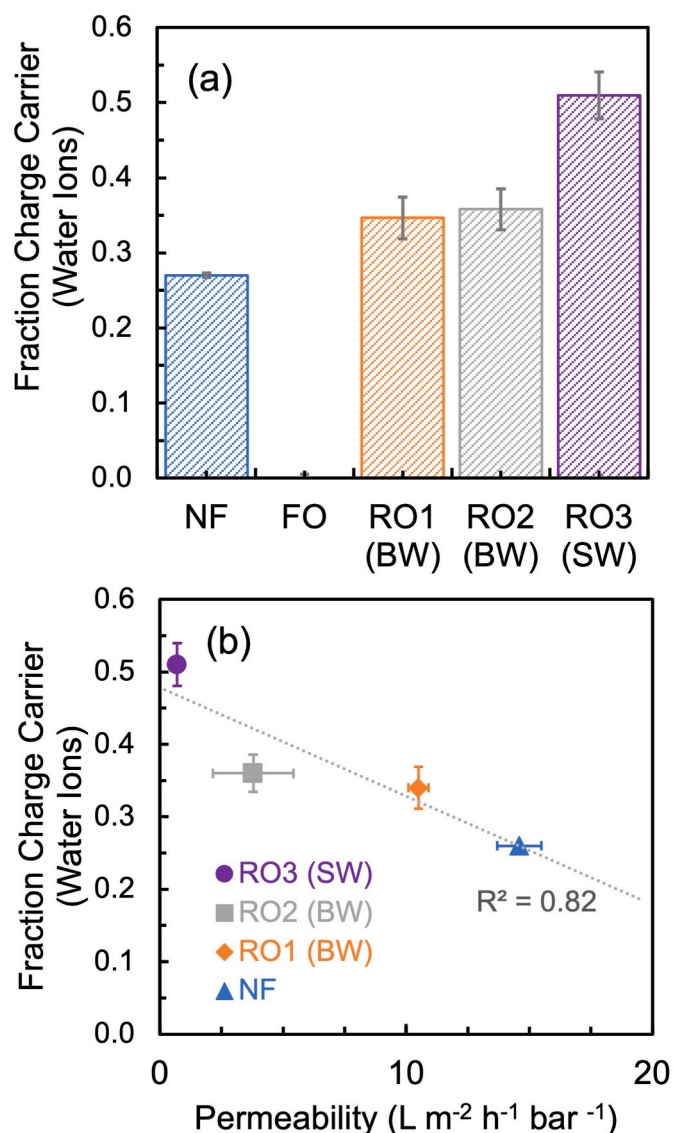

Fig. 5. (a) The fraction of charge that was carried by protons and hydroxide ions for each membrane during the ion crossover experiment. (b) Comparison of the fraction of charge carriers that was protons and hydroxide to the membrane permeability measured using the high-pressure dead-end cell. The equation of the line is $y = -0.01x + 0.48$.

carriers [12]. Because the fraction of charge carrier has a correlation to the membrane water permeability, it seems likely that the membrane polyamide active layer governs large salt ion transport during electrolysis with large pH gradients. In large pH gradients with high concentrations of proton and hydroxide ions, salt ion transport no longer determines the resistance or electrolysis potential because there are preferable, alternative charge carriers (water ions). Therefore, the SWRO membrane, which has the highest reported NaCl rejection [61], contains the salts in their respective compartments the best, and alternatively transports the highest amount of water ions to maintain the current density. The NF membrane, which has the lowest reported NaCl rejection [38,43], allows the most leakage of salt ions between the anolyte and catholyte, and has the least amount of water ions carrying charge. Additional tests will be needed to further examine the significance of this apparent trend.

4. Conclusions

An evaluation of the electrochemical properties of four types of polymeric filtration membranes shows that RO, NF, and FO membrane resistance during electrolysis cannot be predicted using tests developed for ion exchange membranes due to the large pH gradients that will develop in water electrolyzer tests. Results from the ion crossover tests show a general trend of increased charge balance based on water ions rather than salt ions during electrolysis. Charge is balanced by salt ions in resistance tests at neutral pH, while charge is balanced by both salt ions and water ions in water electrolyzer tests. As a result of this higher dependence of water ions in the water electrolyzer tests, there was no correlation between resistances measured at low current densities with overpotentials measured in water electrolyzer tests.

Author's statement

Rachel Taylor: Conceptualization, Methodology, Investigation, Analysis, Writing — Original Draft. **Le Shi:** Conceptualization, Methodology, Analysis, Writing – Reviewing & Editing, Suprervision. **Xuechen Zhou:** Analysis, Writing – Reviewing & Editing. **Ruggero Rossi:** Analysis, Writing – Reviewing & Editing. **Cristian Picioreanu:** Writing – Reviewing & Editing. **Bruce E Logan:** Conceptualization, Methodology, Analysis, Writing – Reviewing & Editing, Supervision.

Declaration of competing interest

The authors declare that they have no known competing financial interests or personal relationships that could have appeared to influence the work reported in this paper.

Data availability

Data will be made available on request.

Acknowledgements

Appendix A. Supplementary data

Supplementary data to this article can be found online at https://doi.org/10.1016/j.memsci.2023.121692.

References

[1] S. Dresp, F. Dionigi, M. Klingenhof, P. Strasser, Direct electrolytic splitting of seawater: opportunities and challenges, ACS Energy Lett. 4 (2019) 933–942, https://doi.org/10.1021/acsenergylett.9b00220.

[2] B.E. Logan, L. Shi, R. Rossi, Enabling the use of seawater for hydrogen gas production in water electrolyzers, Joule 5 (2021) 760–762, https://doi.org/10.1016/j.joule.2021.03.018.

[3] W.M. Tong, M. Forster, F. Dionigi, S. Dresp, R.S. Erami, P. Strasser, A.J. Cowan, P. Farras, Electrolysis of low-grade and saline surface water, Nat. Energy 5 (2020) 367–377, https://doi.org/10.1038/s41560-020-0550-8.

[4] K. Meier, Hydrogen production with sea water electrolysis using Norwegian offshore wind energy potentials, Int. J. Energy Environ. Eng. 5 (2014), https://doi.org/10.1007/s40095-014-0104-6.

[5] R. d'Amore-Domenech, O. Santiago, T.J. Leo, Multicriteria analysis of seawater electrolysis technologies for green hydrogen production at sea, Renew. Sustain. Energy Rev. 133 (2020), https://doi.org/10.1016/j.rser.2020.110166.

[6] Y. Yang, J. Shin, J.T. Jasper, M.R. Hoffmann, Multilayer heterojunction anodes for saline wastewater treatment: design strategies and reactive species generation mechanisms, Environ. Sci. Technol. 50 (2016) 8780–8787, https://doi.org/10.1021/acs.est.6b00688.

[7] E. Asghari, M.I. Abdullah, F. Foroughi, J.J. Lamb, B.G. Pollet, Advances, opportunities, and challenges of hydrogen and oxygen production from seawater electrolysis: an electrocatalysis perspective, Curr. Opin. Electroche. 31 (2022), https://doi.org/10.1016/j.coelec.2021.100879.

[8] F. Dionigi, T. Reier, Z. Pawolek, M. Gliech, P. Strasser, Design criteria, operating conditions, and nickel-iron hydroxide catalyst materials for selective seawater electrolysis, ChemSusChem 9 (2016) 962–972, https://doi.org/10.1002/cssc.201501581.

[9] S. Dresp, F. Dionigi, S. Loos, J.F. de Araujo, C. Spori, M. Gliech, H. Dau, P. Strasser, Direct electrolytic splitting of seawater: activity, selectivity, degradation, and recovery studied from the molecular catalyst structure to the electrolyzer cell level, Adv. Energy Mater. 8 (2018), https://doi.org/10.1002/aenm.201800338.

[10] S. Dresp, T.N. Thanh, M. Klingenhof, S. Bruckner, P. Hauke, P. Strasser, Efficient direct seawater electrolysers using selective alkaline NiFe-LDH as OER catalyst in asymmetric electrolyte feeds, Energy Environ. Sci. 13 (2020) 1725–1729, https://doi.org/10.1039/d0ee01125h.

[11] J.S. Ko, J.K. Johnson, P.I. Johnson, Z.Y. Xia, Decoupling oxygen and chlorine evolution reactions in seawater using iridium-based electrocatalysts, ChemCatChem 12 (2020) 4526–4532, https://doi.org/10.1002/cctc.202000653.

[12] L. Shi, R. Rossi, M. Son, D.M. Hall, M.A. Hickner, C.A. Gorski, B.E. Logan, Using reverse osmosis membranes to control ion transport during water electrolysis, Energy Environ. Sci. 13 (2020) 3138–3148, https://doi.org/10.1039/d0ee02173c.

[13] P.M. Biesheuvel, L. Zhang, P. Gasquet, B. Blankert, M. Elimelech, W.G.J. van der Meer, Ion selectivity in brackish water desalination by reverse osmosis: theory, measurements, and implications, Environ. Sci. Technol. Lett. 7 (2020) 42–47, https://doi.org/10.1021/acs.estlett.9b00686.

[14] V. Freger, G.Z. Ramon, Polyamide desalination membranes: formation, structure, and properties, Prog. Polym. Sci. 122 (2021), https://doi.org/10.1016/j.progpolymsci.2021.101451.

[15] N. Fridman-Bishop, V. Freger, What makes aromatic polyamide membranes superior: new insights into ion transport and membrane structure, J. Membr. Sci. 540 (2017) 120–128, https://doi.org/10.1016/j.memsci.2017.06.035.

[16] M. Hafiz, A.H. Hawari, R. Alfahel, M.K. Hassan, A. Altaee, Comparison of nanofiltration with reverse osmosis in reclaiming tertiary treated municipal wastewater for irrigation purposes, Membr. Biochem. 11 (2021), https://doi.org/10.3390/membranes11010032.

[17] J. Benavente, C. Fernandezpineda, Electrokinetic phenomena in porous membranes - determination of phenomenological coefficients and transport numbers, J. Membr. Sci. 23 (1985) 121–136, https://doi.org/10.1016/S0376-7388(00)82214-0.

[18] G. Jonsson, J. Benavente, Determination of some transport-coefficients for the skin and porous layer of a composite membrane, J. Membr. Sci. 69 (1992) 29–42, https://doi.org/10.1016/0376-7388(92)80165-G.

[19] J. Benavente, G. Jonsson, Electrokinetic characterization of composite membranes: estimation of different electrical contributions in pressure induced potential measured across reverse osmosis membranes, J. Membr. Sci. 172 (2000) 189–197, https://doi.org/10.1016/S0376-7388(00)00325-2.

[20] L. Lin, C.C. Feng, R. Lopez, O. Coronell, Identifying facile and accurate methods to measure the thickness of the active layers of thin-film composite membranes - a comparison of seven characterization techniques, J. Membr. Sci. 498 (2016) 167–179, https://doi.org/10.1016/j.memsci.2015.09.059.

[21] S. Habib, S.T. Weinman, A review on the synthesis of fully aromatic polyamide reverse osmosis membranes, Desalination 502 (2021), https://doi.org/10.1016/j.desal.2021.114939.

[22] R.J. Petersen, Composite reverse-osmosis and nanofiltration membranes, J. Membr. Sci. 83 (1993) 81–150, https://doi.org/10.1016/0376-7388(93)80014-O.

[23] D.L. Shaffer, J.R. Werber, H. Jaramillo, S.H. Lin, M. Elimelech, Forward osmosis: where are we now? Desalination 356 (2015) 271–284, https://doi.org/10.1016/j.desa12014.10.031.

[24] A.H. Galama, N.A. Hoog, D.R. Yntema, Method for determining ion exchange membrane resistance for electrodialysis systems, Desalination 380 (2016) 1–11, https://doi.org/10.1016/j.desal.2015.11.018.

[25] G.J. Hwang, H. Ohya, T. Nagai, Ion exchange membrane based on block copolymers. Part III: preparation of cation exchange membrane, J. Membr. Sci. 156 (1999) 61–65, https://doi.org/10.1016/S0376-7388(98)00331-7.

[26] J. Kamcev, R. Sujanani, E.S. Jang, N. Yan, N. Moe, D.R. Paul, B.D. Freeman, Salt concentration dependence of ionic conductivity in ion exchange membranes, J. Membr. Sci. 547 (2018) 123–133, https://doi.org/10.1016/j.memsci.2017.10.024.

[27] N. Fridman-Bishop, V. Freger, When salt-rejecting polymers meet protons: an electrochemical impedance spectroscopy investigation, Langmuir 33 (2017) 1391–1397, https://doi.org/10.1021/acs.langmuir.6b04263.

[28] M. Stolov, V. Freger, Membrane charge weakly affects ion transport in reverse osmosis, Environ. Sci. Technol. Lett. 7 (2020) 440–445, https://doi.org/10.1021/acs.estlett.0c00291.

[29] M. Stolov, V. Freger, Degradation of polyamide membranes exposed to chlorine: an impedance spectroscopy study, Environ. Sci. Technol. 53 (2019) 2618–2625, https://doi.org/10.1021/acs.est.8b04790.

[30] G. Tiravanti, The direct-current method for measuring charged membrane conductance, J. Membr. Sci. 9 (1981) 229–243, https://doi.org/10.1016/S0376-7388(00)80266-5.

[31] G.M. Geise, A.J. Curtis, M.C. Hatzell, M.A. Hickner, B.E. Logan, Salt concentration differences alter membrane resistance in reverse electrodialysis stacks, Environ. Sci. Technol. Lett. 1 (2014) 36–39, https://doi.org/10.1021/ez4000719.

[32] W. Oelssner, F. Berthold, U. Guth, The iR drop - well-known but often underestimated in electrochemical polarization measurements and corrosion

testing, Mater. Corros. 57 (2006) 455–466, https://doi.org/10.1002/maco.200603982.

[33] M. Arif, S.C.P. Cheung, J. Andrews, A systematic approach for matching simulated and experimental polarization curves for a PEM fuel cell, Int. J. Hydrogen Energy 45 (2020) 2206–2223, https://doi.org/10.1016/j.ijhydene.2019.11.057.

[34] M. Carmo, D.L. Fritz, J. Merge, D. Stolten, A comprehensive review on PEM water electrolysis, Int. J. Hydrogen Energy 38 (2013) 4901–4934, https://doi.org/10.1016/j.ijhydene.2013.01.151.

[35] R. Phillips, C.W. Dunnill, Zero gap alkaline electrolysis cell design for renewable energy storage as hydrogen gas, RSC Adv. 6 (2016) 100643–100651, https://doi.org/10.1039/c6ra22242k.

[36] Y. Okamoto, J.H. Lienhard, How RO membrane permeability and other performance factors affect process cost and energy use: a review, Desalination 470 (2019), https://doi.org/10.1016/j.desal.2019.07.004.

[37] R. Epsztein, R.M. DuChanois, C.L. Ritt, A. Noy, M. Elimelech, Towards single-species selectivity of membranes with subnanometre pores, Nat. Nanotechnol. 15 (2020) 426–436, https://doi.org/10.1038/s41565-020-0713-6.

[38] C. Boo, Y.K. Wang, I. Zucker, Y. Choo, C.O. Osuji, M. Elimelech, High performance nanofiltration membrane for effective removal of perfluoroalkyl substances at high water recovery, Environ. Sci. Technol. 52 (2018) 7279–7288, https://doi.org/10.1021/acs.est.8b01040.

[39] TriSep ACM5 Low Energy RO Membrane, Product specification - Trisep ACM5," TriSep [Online]. Available: https://www.lenntech.com/Data-sheets/Trisep-2540-ACM5-TSF-L.pdf, 2021.

[40] S.N. Lvov, Introduction to electrochemical science and engineering. p. 1 online resource.

[41] T.E. Culp, Y.X. Shen, M. Geitner, M. Paul, A. Roy, M.J. Behr, S. Rosenberg, J. Gu, M. Kumar, E.D. Gomez, Electron tomography reveals details of the internal microstructure of desalination membranes, Proc. Natl. Acad. Sci. USA 115 (2018) 8694–8699, https://doi.org/10.1073/pnas.1804708115.

[42] V. Kolev, V. Freger, Hydration, porosity and water dynamics in the polyamide layer of reverse osmosis membranes: a molecular dynamics study, Polymer 55 (2014) 1420–1426, https://doi.org/10.1016/j.polymer.2013.12.045.

[43] N. Hilal, H. Al-Zoubi, A.W. Mohammad, N.A. Darwish, Nanofiltration of highly concentrated salt solutions up to seawater salinity, Desalination 184 (2005) 315–326, https://doi.org/10.1016/j.desal.2005.02.062.

[44] J. Wei, C.Q. Qiu, C.Y.Y. Tang, R. Wang, A.G. Fane, Synthesis and characterization of flat-sheet thin film composite forward osmosis membranes, J. Membr. Sci. 372 (2011) 292–302, https://doi.org/10.1016/j.memsci.2011.02.013.

[45] J. Wei, Q.H. She, X. Liu, Insights into the influence of membrane permeability and structure on osmotically-driven membrane processes, Membr. Biochem. 11 (2021), https://doi.org/10.3390/membranes11020153.

[46] J.C. Diaz, J. Kamcev, Ionic conductivity of ion-exchange membranes: measurement techniques and salt concentration dependence, J. Membr. Sci. 618 (2021), https://doi.org/10.1016/j.memsci.2020.118718.

[47] J. Hnat, M. Plevova, J. Zitka, M. Paidar, K. Bouzek, Anion-selective materials with 1,4-diazabicyclo[2.2.2]octane functional groups for advanced alkaline water electrolysis, Electrochim. Acta 248 (2017) 547–555, https://doi.org/10.1016/j.electacta.2017.07.165.

[48] A. Ramdani, A. Deratani, S. Taleb, N. Drouiche, H. Lounici, Performance of NF90 and NF270 commercial nanofiltration membranes in the defluoridation of Algerian brackish water, Desalination Water Treat. 212 (2021) 286–296, https://doi.org/10.5004/dwt.2021.26680.

[49] M. Manttari, T. Pekuri, M. Nystrom, NF270, a new membrane having promising characteristics and being suitable for treatment of dilute effluents from the paper industry, J. Membr. Sci. 242 (2004) 107–116, https://doi.org/10.1016/j.memsci.2003.08.032.

[50] K. Kosutic, L. Kastelan-Kunst, B. Kunst, Porosity of some commercial reverse osmosis and nanofiltration polyamide thin-film composite membranes, J. Membr. Sci. 168 (2000) 101–108, https://doi.org/10.1016/S0376-7388(99)00309-9.

[51] Product data sheet FilmTec NF270 nanofiltration elements for commercial systems, DuPont [Online]. Available: https://www.dupont.com/content/dam/dupont/amer/us/en/water-solutions/public/documents/en/NF-FilmTec-NF270-PDS-45-D01529-en.pdf, 2021.

[52] Z.Y. Wang, Z.X. Wang, S.H. Lin, H.L. Jin, S.J. Gao, Y.Z. Zhu, J. Jin, Nanoparticle-templated nanofiltration membranes for ultrahigh performance desalination, Nat. Commun. 9 (2018), https://doi.org/10.1038/s41467-018-04467-3.

[53] L.F. Greenlee, D.F. Lawler, B.D. Freeman, B. Marrot, P. Moulin, Reverse osmosis desalination: water sources, technology, and today's challenges, Water Res. 43 (2009) 2317–2348, https://doi.org/10.1016/j.watres.2009.03.010.

[54] K.R. Cooper, M. Smith, Electrical test methods for on-line fuel cell ohmic resistance measurement, J. Power Sources 160 (2006) 1088–1095, https://doi.org/10.1016/j.jpowsour.2006.02.086.

[55] OsmoF2OTM Forward Osmosis Membranes Flat Sheet Membranes, Fluid Technology Solutions, Inc., 2018 [Online]. Available: https://www.sterlitech.com/media/wysiwyg/FTS_Data_Sheet.pdf.

[56] DuPont, FilmTech XLE-440 element, in: Product Data Sheet, 2020 [Online]. Available: https://www.dupont.com/content/dam/dupont/amer/us/en/water-solutions/public/documents/en/RO-FilmTec-XLE-440-PDS-45-D01513-en.pdf.

[57] G. Li, X.M. Li, T. He, B. Jiang, C.J. Gao, Cellulose triacetate forward osmosis membranes: preparation and characterization, Desalination Water Treat. 51 (2013) 2656–2665, https://doi.org/10.1080/19443994.2012.749246.

[58] L. Wang, T.C. Cao, J.E. Dykstra, S. Porada, P.M. Biesheuvel, M. Elimelech, Salt and water transport in reverse osmosis membranes: beyond the solution-diffusion model, Environ. Sci. Technol. 55 (2021) 16665–16675, https://doi.org/10.1021/acs.est.1c05649.

[59] R. Epsztein, E. Shaulsky, N. Dizge, D.M. Warsinger, M. Elimelech, Role of ionic charge density in Donnan exclusion of monovalent anions by nanofiltration, Environ. Sci. Technol. 52 (2018) 4108–4116, https://doi.org/10.1021/acs.est.7b06400.

[60] S.J. Kim, S. Kook, B.E. O'Rourke, J. Lee, M. Hwang, Y. Kobayashi, R. Suzuki, I.S. Kim, Characterization of pore size distribution (PSD) in cellulose triacetate (CTA) and polyamide (PA) thin active layers by positron annihilation lifetime spectroscopy (PALS) and fractional rejection (FR) method, J. Membr. Sci. 527 (2017) 143–151, https://doi.org/10.1016/j.memsci.2016.12.064.

[61] Hydranautics, SWC4-LD" Hydranautics Nitto Group Company, 2018.